



Citation for published version:

Irikura, K, Marken, F, Fletcher, P, Kociok-Kohn, G & Zanoni, MVB 2020, 'Direct and Indirect Light Energy Harvesting with Films of Ambiently Deposited ZnO Nanoparticles', *Applied Surface Science*, vol. 527, 146927. <https://doi.org/10.1016/j.apsusc.2020.146927>

DOI:

[10.1016/j.apsusc.2020.146927](https://doi.org/10.1016/j.apsusc.2020.146927)

Publication date:

2020

Document Version

Peer reviewed version

[Link to publication](#)

Publisher Rights

CC BY-NC-ND

University of Bath

Alternative formats

If you require this document in an alternative format, please contact:
openaccess@bath.ac.uk

General rights

Copyright and moral rights for the publications made accessible in the public portal are retained by the authors and/or other copyright owners and it is a condition of accessing publications that users recognise and abide by the legal requirements associated with these rights.

Take down policy

If you believe that this document breaches copyright please contact us providing details, and we will remove access to the work immediately and investigate your claim.

1
2
3
4
5
6
7
8
9
10
11
12
13
14
15
16
17
18
19
20
21
22
23
24
25
26
27
28

REVISION

Direct and Indirect Light Energy Harvesting with Films of Ambiently Deposited ZnO Nanoparticles

Kallyni Irikura ^{a,b,c,*}, Frank Marken ^c, Philip J. Fletcher ^d, Gabriele Kociok-Köhn ^d,
and Maria Valnice Boldrin Zanoni ^{a,b}

^a *São Paulo State University (Unesp), Institute of Chemistry, Araraquara*

^b *National Institute of Alternative Technologies for Detection, Toxicological Evaluation and Removal of Micropollutants and Radioactive Substances (INCT-DATREM), São Paulo State University (Unesp), Institute of Chemistry, Araraquara*

^c *University of Bath, Department of Chemistry, Bath BA2 7AY, UK*

^d *University of Bath, Materials and Chemical Characterisation Facility MC², Bath BA2 7AY, UK*

To be submitted to Applied Surface Science

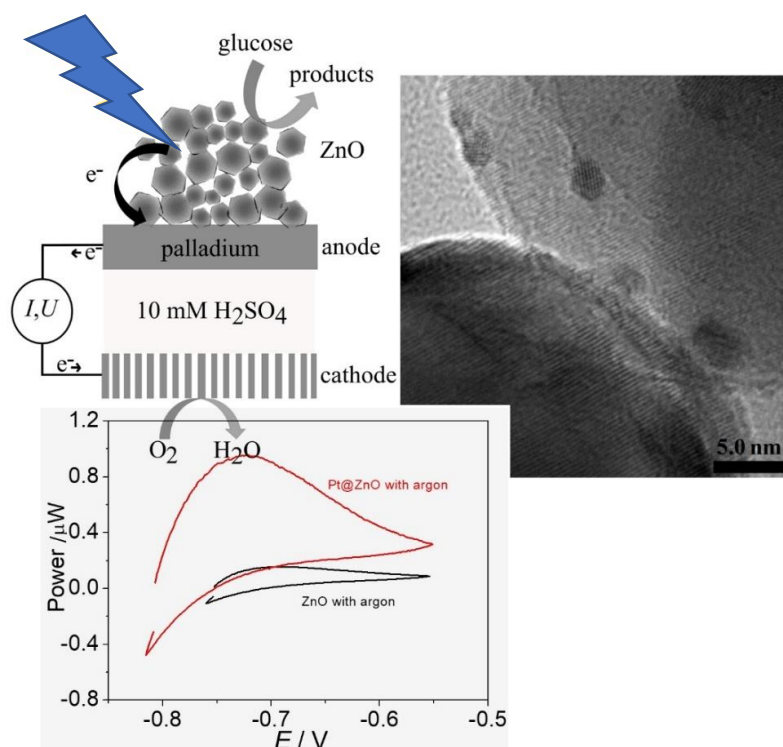
*Corresponding author. Tel.: +55 16 33019740; E-mail address: kallyni.irikura@unesp.br or kallyni@gmail.com

Abstract

29 Indirect photoelectrochemical processes are possible when employing a palladium film
30 to separate photochemical and electrochemical reactions. Here, an exploratory indirect
31 photoelectrochemical system is developed based on ZnO or Pt@ZnO nanoparticle
32 photocatalysts ambiently deposited onto platinum, glassy carbon, or palladium membrane
33 electrodes and exposed to blue (385 nm) LED light in the presence of glucose hole quencher
34 (in aqueous NaCl). It is demonstrated that under these conditions photo-excitation followed by
35 charge transport of conduction band electrons via inter-grain conduction across ZnO particles
36 triggers the photo-current responses. The conduction band electrons then trigger formation of
37 interstitial hydrogen in a palladium membrane. Transport of the hydrogen across the palladium
38 membrane into the electrochemical compartment occurs within 1-2 minutes of switching on
39 the light. A proof-of-principle fuel cell with oxygen gas diffusion electrode (cathode) and
40 indirect photo-anode is shown to operate with up to $28 \mu\text{W cm}^{-2}$ power output during
41 illumination. Important power-limiting parameters and suggestions for future improvements
42 are discussed.

43

44 Graphical abstract



45

46 **Keywords:** ZnO nanoparticles, Pt@ZnO, palladium membrane, photocatalytic hydrogen
47 generation, glucose

48

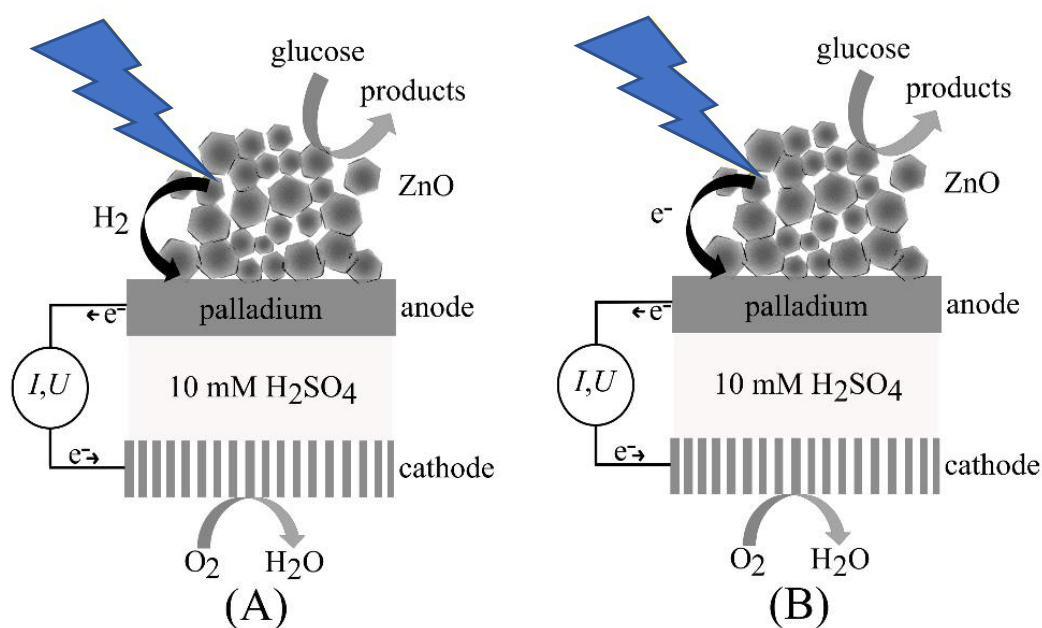
49 1. Introduction

50 Hydrogen is a gaseous energy-vector widely used in various industrial fields [1,2]. In
51 the petroleum industry hydrogen is used in processes such as hydrocracking, hydro-
52 desulfurization and hydro-dealkylation [3,4]. Nowadays, hydrogen produced from renewable
53 resources has been identified as a sustainable alternative energy carrier to relieve
54 environmental problems and to lower the dependence on conventional fossil fuels. In
55 particular, hydrogen used in proton exchange membrane fuel cells is attractive due the
56 efficiency of the energy conversion without the release of greenhouse gases [4]. In contrast to
57 processes based on bulk-scale hydrogen, it is possible to also employ hydrogen as energy-
58 vector on microscopic scale coupled for example to photocatalysis.

59
60 In this study, we used a commercial nano-ZnO photocatalyst (MZ-300, Tayca, Japan)
61 with nominally 35 nm diameter and 30 m²g⁻¹ surface area [5]. ZnO exhibits unique physical
62 and (photo-)chemical properties and a band gap in the near ultraviolet [6,7]. However, it is
63 known that the photo-current generation efficiency of ZnO can be low due to a high
64 recombination rate of the photo-generated e⁻/h⁺ pairs [8,9]. To enhance the photocatalytic
65 performance of the ZnO either hole quenchers can be added and/or photo-deposition of
66 platinum nanoparticles has been suggested to help improve the charge separation and the
67 hydrogen evolution reaction [10,11].

68
69 Recently, the concept of an indirectly driven photoelectrochemical process has been
70 proposed [12] based on the idea of separating the photoelectrochemical process and the
71 electrolytic process with a thin palladium membrane. The key benefit of the indirect *versus* the
72 direct photoelectrochemical process is in the possibility to employ different solution
73 compositions for photocatalysis (e.g. with biomass) and for electrochemical energy conversion
74 (e.g. with pure mineral acids). Hydrogen provides the “micro-energy vector” connecting
75 photocatalysis through hydrogen-permeable palladium with the electrochemical reaction. The
76 concept is based on a photo-redox process producing hydrogen at the surface of nanoparticles
77 (e.g. for Pt@g-C₃N₄ [12] or here for Pt@ZnO [13]) deposited onto a palladium membrane.
78 Under illumination and in the presence of glucose hole quencher, hydrogen is produced locally
79 as energy carrier and transported towards a palladium membrane where hydrogen is readily
80 absorbed. Once bound into palladium, the hydrogen can be transferred to the opposite side of
81 the film and released in an electrochemical process [4,14,15]. This happens in contact with

82 electrolyte solution, where discharge of hydrogen produces protons (in aqueous acid). This
 83 anodic process can be coupled to a cathodic gas diffusion electrode where oxygen is reduced
 84 (see Fig. 1). Overall, the photo-redox process in the presence of a quencher such as glucose
 85 (here chosen to represent biomass) can be shown to transform power via hydrogen transport
 86 through palladium [16].
 87



88
 89 **Figure 1** – Schematic illustration of an indirectly driven photoelectrochemical cell based on
 90 (A) hydrogen generation and transfer to a palladium membrane and (B) electron generation
 91 and transfer to a palladium membrane.

92
 93 A peculiar mechanistic issue arises for this type of reaction sequence when either the
 94 production of hydrogen (see Figure 1A) or the production of electrons (see Figure 1B) can be
 95 responsible for the uptake of hydrogen into the palladium membrane. Although the mechanism
 96 based on hydrogen may appear more plausible, it is shown here that in fact the mechanism
 97 based on electronic transport appears to dominate for ZnO. Ambiently deposited ZnO
 98 nanoparticles are investigated (and compared to Pt@ZnO nanoparticles) and transport via
 99 electron hopping is shown to be effective without sintering of the ZnO nanoparticles. Factors
 100 such as surface conductivity, surface poisoning, glucose concentration, substrate effects, and
 101 electrolyte effects are considered. In addition to the previous reports on indirect
 102 photoelectrochemical processes [12], this constitutes a new case at the level of proof-of-
 103 principle.

104

105 **2. Experimental**

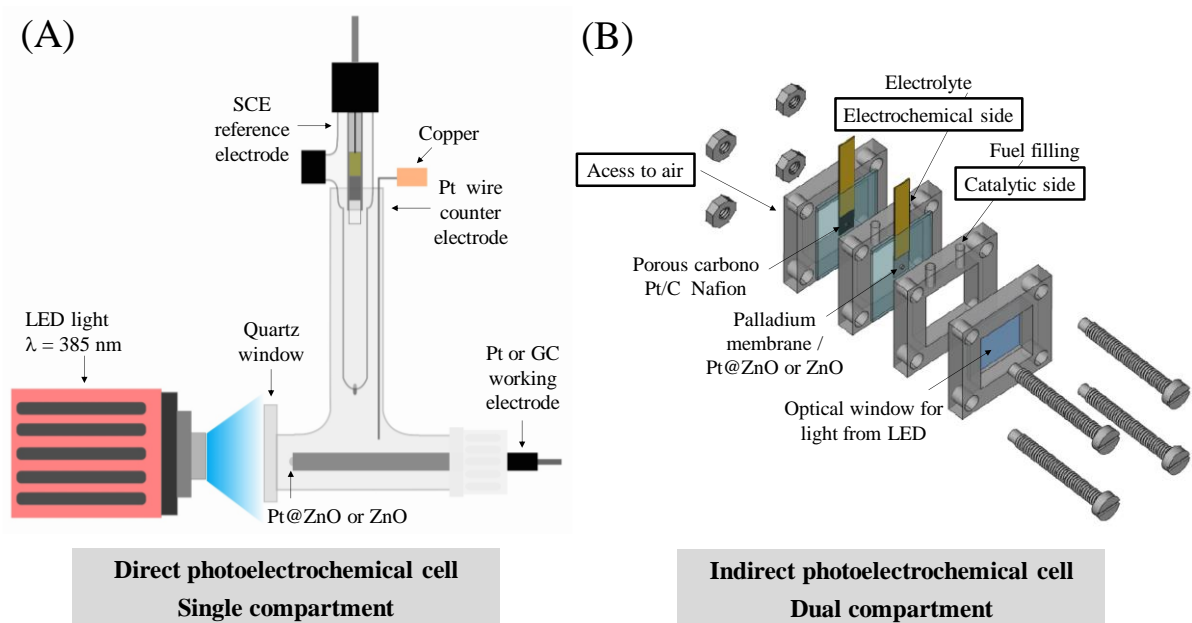
106 **2.1. Chemical Reagents.** All reagents were used without further purification. Deionised water
107 (CE Instruments Ltd ultra-pure water system 18.2 M Ω cm at 22 \pm 2 $^{\circ}$ C) was used for the
108 preparation of all solutions.

109
110 **2.2. Procedure for Pt@ZnO.** The Pt@ZnO powder was produced from of mixture containing
111 20 mg ZnO (Tayca Corporation MZ-300 lot N. 300194) and 0.3 mg K₂PtCl₆ (Sigma-Aldrich)
112 dispersed in 20 mL H₂O and 2 mL methanol (VWR Chemicals). This mixture was inserted in
113 a glass container with magnetic stirring and illuminated for 20 h using a power LED (λ = 385,
114 ca. 100 mWcm⁻², Thorlabs, UK). The coloration of ZnO changes from white to grey. After of
115 the synthesis of the Pt@ZnO, it was separated, washed with ethanol, centrifuged (Eppendorf
116 5804-R) and dried at room temperature. Heat treatments were performed at 200 $^{\circ}$ C and at
117 400 $^{\circ}$ C in an open tube furnace (Elite Thermal Systems Ltd TSH 12/65/550) for 2h.

118
119 **2.3. Instrumentation.** The characteristic powder patterns in the 2θ range from of 20 $^{\circ}$ to 95 $^{\circ}$
120 were obtained by X-ray diffraction (PXRD) with a STADI P system with Cu K α 1 radiation
121 (1.5406 \AA). Transmission electron microscopy (TEM) images were obtained with a JEOL
122 JEM-2100Plus system equipped with an Oxford Instruments X-Max^N TSR Windowless
123 Energy dispersive X-ray analyser (EDX).

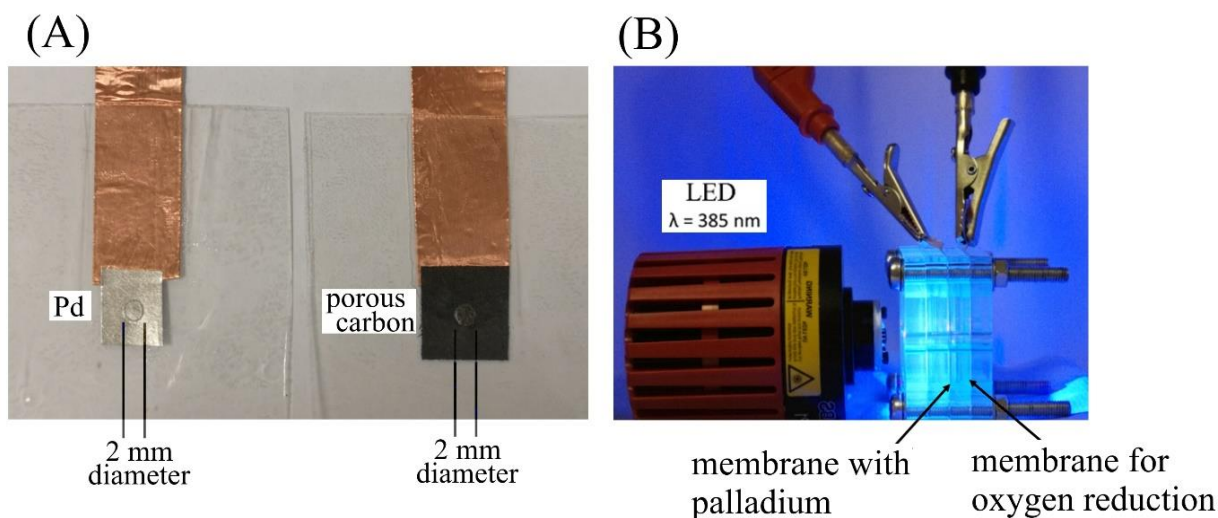
124
125 Electrochemical measurements were performed with an Autolab PGSTAT using GPES
126 software (Metrohm, UK). Cyclic voltammetry measurements were carried out over a potential
127 range from +0.6 V to -0.8 V vs. SCE and with a scan rate of 50 mV s⁻¹ without and with
128 application of pulsed light (1 s off and 2 s on) using a power LED (λ = 385, approx. 100 mWcm⁻
129 ², Thorlabs, UK). For initial measurements at platinum or glassy carbon disk electrodes (3 mm
130 diameter, BASi), a three-electrode cell was employed with a saturated calomel (SCE,
131 Radiometer, Copenhagen) reference electrode and a platinum wire counter electrode (Advent
132 Materials, UK) as illustrated in the Fig. 2A. The working electrode was prepared by deposition
133 of a volume of 2-16 μ L of a mixture of 6 mg of ZnO or Pt@ZnO in 1 mL of 1:1 v/v ethanol
134 (VWR Chemicals) and H₂O.

135



136
137
138
139
140
141
142
143

Figure 2 – (A) Experimental system for three-electrode measurements (platinum disk working electrode, SCE reference, Pt wire counter electrode) with a single compartment for the photoelectrochemical measurements. (B) Schematic drawing of the 3D-printed cell for two-electrode measurements with a fuel or catalysis side for the photochemical process, a palladium membrane/working electrode to allow transport of hydrogen, an electrochemical compartment with electrolyte, and an oxygen breathing gas diffusion electrode.



144
145
146
147
148

Figure 3 – (A) Laminated film electrodes based on 0.025 mm thickness palladium and 0.11 mm thickness porous carbon (Toray 030). (B) Photographic image of the illuminated 3D-printed two-compartment indirect photo-electrochemical cell.

149 Zero current chronopotentiometry and chronoamperometry experiments were
150 performed in an indirect photo-fuel cell according to the illustration in Fig. 2B. The electrodes
151 were prepared using copper tape to provide electric contact and thermal lamination film
152 (polypropylene film) to leave exposed only an area of 2 mm diameter on both sides and for

153 both types of electrodes. Porous carbon (Toray Paper 030, see Fig. 3A) was used as cathode
154 and modified with 6 μL of a mixture of 5 mg Pt/C catalyst (HISPEC 4000, Johnson Matthey,
155 40 wt% Pt) dispersed in 1 mL isopropanol and 2 μL of Nafion 117 solution (5 wt%, Aldrich)
156 to improve the proton mobility when the oxygen is reduced and to keep the catalyst on the
157 carbon membrane. As anode was used palladium membrane (Goodfellow, 0.025 mm thickness,
158 optically tested) modified with 4 μL of the mixture of ZnO or Pt@ZnO dispersed in
159 ethanol/H₂O (usually 6 mg solid per mL of ethanol/H₂O 1:1). A solution of 10 mmol L⁻¹ H₂SO₄
160 was inserted in the electrochemical compartment and a solution of 500 mmol L⁻¹ glucose in 10
161 mmol L⁻¹ NaCl was filled into the catalytic compartment. Measurements were conducted at
162 open circuit potential (OCP), with light irradiation ($\lambda = 385 \text{ nm}$) for 950s, either in ambient air
163 or with argon de-aeration. Subsequently, cyclic voltammetry measurements were carried out
164 starting at OCP with a scan rate of 1 mV s⁻¹ to give information about the fuel cell power
165 generation.

166

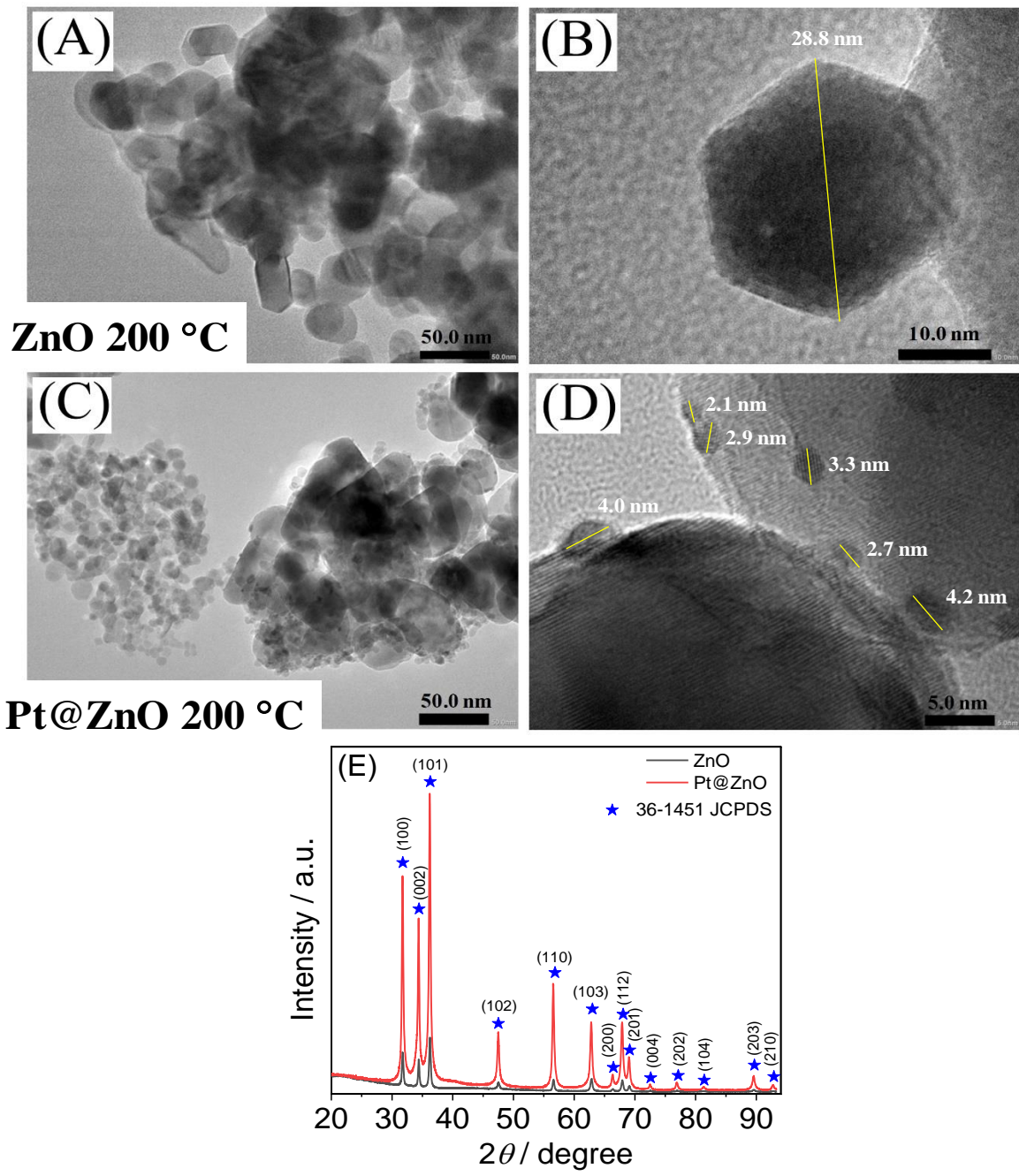
167 **3. Results and Discussion**

168 **3.1. Production and Characterisation of ZnO and Pt@ZnO Nanophotocatalysts**

169 ZnO and Pt@ZnO materials were employed with and without initial heat treatment to
170 make photo-electrochemical experiments more reproducible. A mild 200 °C heat treatment
171 seemed to give the most encouraging results (*vide infra*; also see data in Fig. S1). The
172 morphology of the ZnO or Pt@ZnO powders with 2 h heat treatment at 200 °C in air was
173 characterised by TEM (additional data for materials without heat treatment with 200 °C and
174 400 °C treatment are essentially identical as shown in Fig. S2). In Fig. 4A and 4B a mixed
175 morphology can be seen with spherical, hexagonal and elongated hexagonal shapes, which
176 suggest some aggregation and particle diameters of typically 29 nm (close to the nominal
177 particle size, 35 nm, for this commercial nano-material). With platinum nanoparticles “photo-
178 attached” onto the ZnO nanoparticles (by photoconversion of Pt⁴⁺ to Pt⁰ when stirring a
179 suspension of ZnO and K₂PtCl₆, see experimental) a grey powder (in contrast to white ZnO) is
180 obtained. Formation of platinum is confirmed in Fig. 4C as dark dots attached to the ZnO with
181 an average particle size of 3.2 nm (Fig. 4D). XRD measurements were performed (see Fig. 4E)
182 in order to determine the crystalline phase of these materials. For both materials ZnO and
183 Pt@ZnO the same diffraction peaks for the hexagonal wurtzite phase were confirmed in good
184 agreement with 36-1451 standard data from the JCPDS data base with strong and sharp
185 diffraction peaks at $2\theta = 31.7^\circ, 34.4^\circ, 36.2^\circ, 47.5^\circ, 56.8^\circ, 62.9^\circ, 66.4^\circ, 68.0^\circ, 69.1^\circ, 72.5^\circ,$

186 77.1°, 81.3°, 89.6°, 92.8° corresponding to crystalline planes (100), (002), (101), (102), (110),
 187 (103), (200), (112), (201), (004), (202), (104), (203) and (210), respectively [17]. It is
 188 noteworthy that no diffraction peaks for Pt are detected in the Pt@ZnO material, which is
 189 mainly due to the low volume of Pt and the small crystal size for Pt deposited onto the ZnO
 190 nanoparticles. Similar behaviour also was noted by Li *et al.* [10].

191

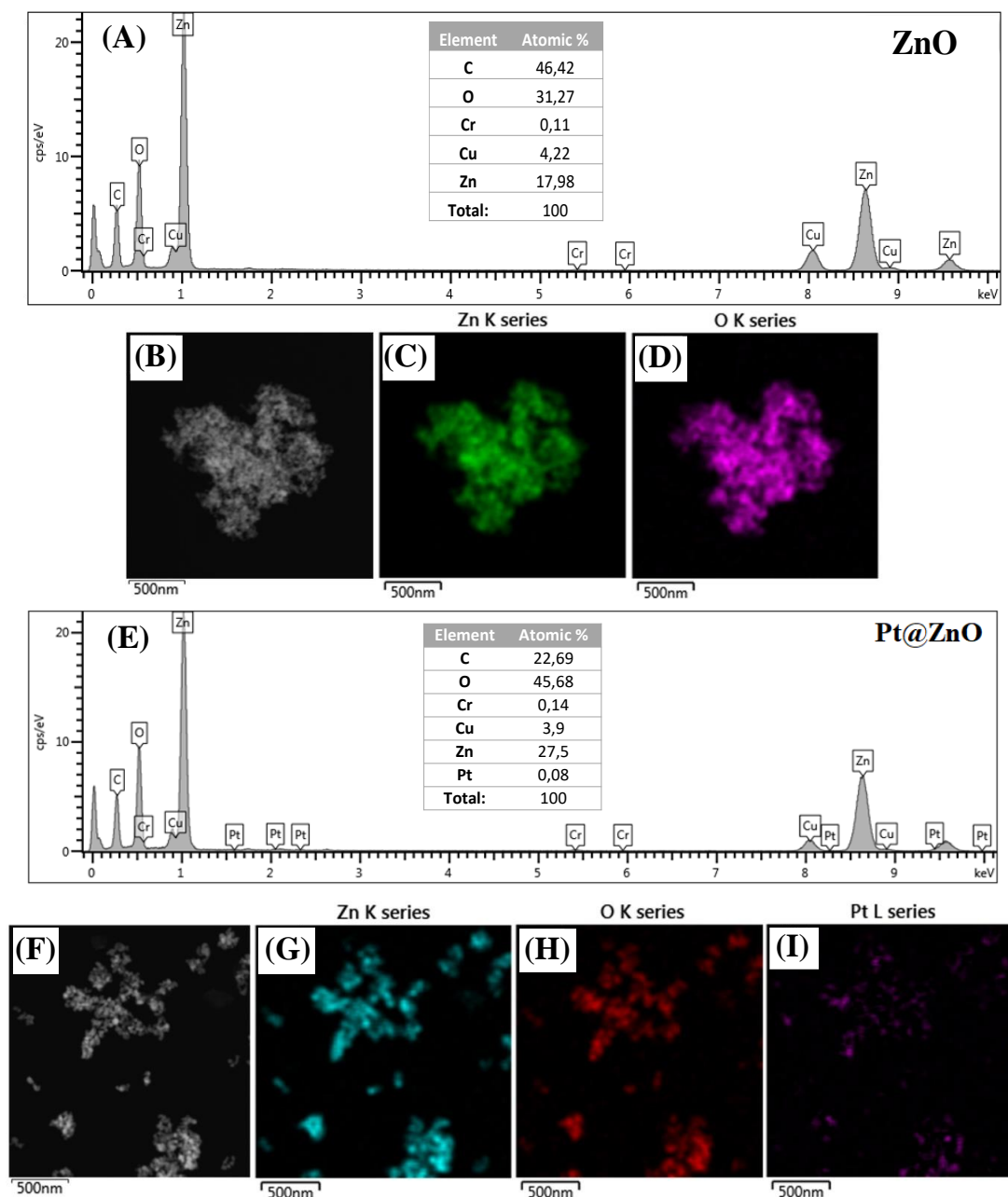


192

193 **Figure 4** – Transmission electron micrograph (TEM) images for ZnO (A, B) and for Pt@ZnO
 194 (C, D); X-ray diffractogram of ZnO and Pt@ZnO (E). Both samples were previously heat
 195 treated at 200 °C.

196
 197
 198
 199
 200
 201
 202

The elemental mappings and composition of the materials were measured by energy dispersive X-ray analysis (EDX) and are shown in the Fig. 5. The spectra in Fig.5A and 5E show in % atomic elements O and Zn (with C, Cr, Cu due to the substrate). Pt is observed in Fig. 5E. Fig. 5B – 5D and Fig. 5F – 5H show elemental mappings for both materials. Nanoparticles of Pt are homogenously distributed over the bigger ZnO nanoparticles.



203
 204
 205

Figure 5 – Energy dispersive X-ray spectroscopy (EDX) data and mapping for the ZnO (A-D) and for Pt@ZnO (E-I).

206

207 **3.2. Photoelectrochemical Characterisation of Pt@ZnO and ZnO Nanophotocatalysts**

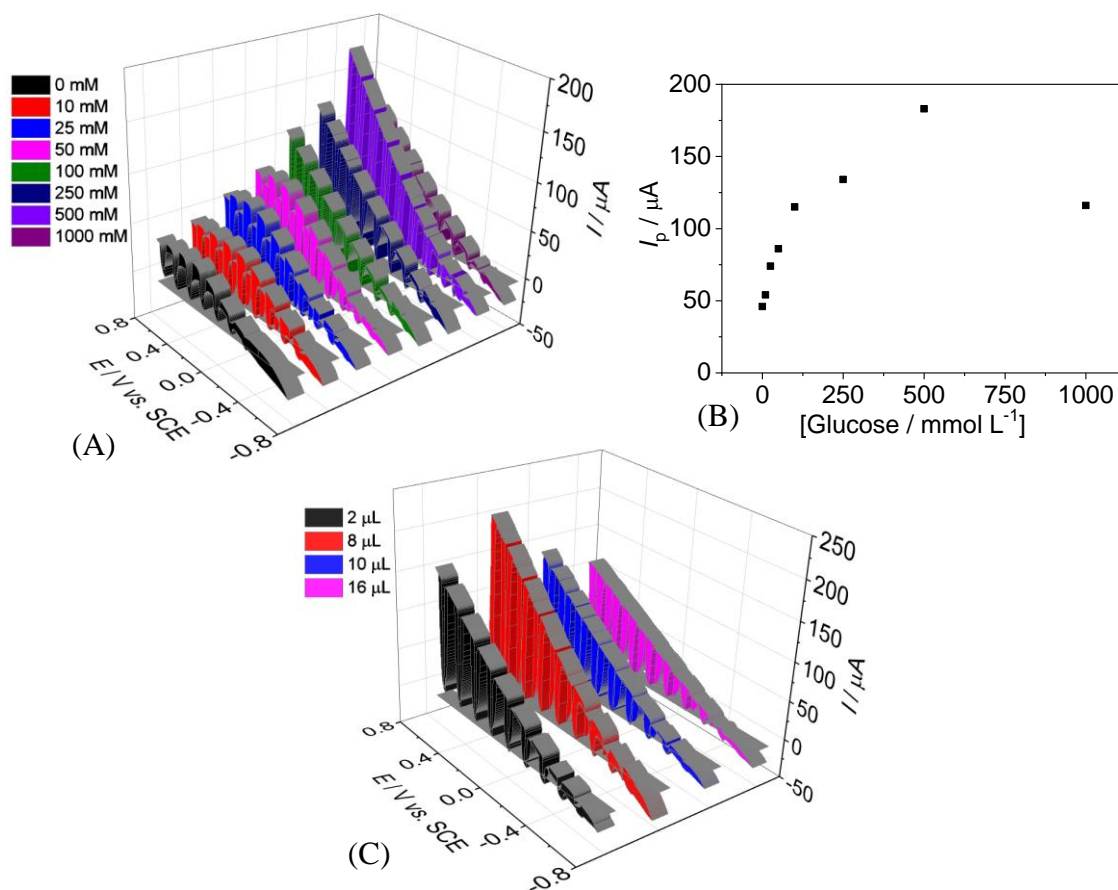
208 In initial photoelectrochemical experiments, the selected electrolyte was 10 mmol L⁻¹
209 phosphate buffer solution at pH 7 containing 500 mmol L⁻¹ glucose as the hole quencher. A
210 volume of 8 μL of Pt@ZnO suspension (48 μg Pt@ZnO) was deposited onto either glassy
211 carbon or platinum disk electrodes. Data in Fig. S3 show that only very poor photo-
212 electrochemical responses are observed for both types of electrodes. For the platinum electrode
213 the photo-electrochemical responses were more significant (Fig. S3B), but also rapidly
214 decaying after three voltammetric cycles. This is tentatively assigned to phosphate-induced
215 inactivation/modification of the Pt@ZnO surface. According to Hermann *et al.* [18], zinc oxide
216 nanoparticles are highly sensitive towards phosphate anions even at pH 7.

217

218 To avoid this problem, the phosphate buffer solution was replaced by aqueous 10 mmol
219 L⁻¹ NaCl. Exploratory experiments were carried out with Pt@ZnO nanoparticles in 10 mmol
220 L⁻¹ NaCl to assess the effects of the amount of deposition and the concentration of glucose hole
221 quencher. Fig. 6A shows cyclic voltammetry data obtained under pulsed light conditions ($\lambda =$
222 385 nm; 1 s off 2 s on; approx. 100 mWcm⁻²) for electrodes immersed in 10 mmol L⁻¹ NaCl
223 with varying concentrations of 0 – 1000 mmol L⁻¹ glucose. The photocatalyst, 48 μg Pt@ZnO,
224 is deposited onto a 3 mm diameter platinum disc electrode and an onset of photocurrents is
225 observed at -0.6 V *vs.* SCE (see Fig. 6A). With a more positive applied voltage, the
226 photocurrent responses increase reaching approx. 190 μA at 0.6 V *vs.* SCE (corresponding to
227 2.7 mAcm⁻²). These are substantial photocurrent responses and the effect of glucose
228 concentration (Fig. 6B) suggests that glucose acts as a quencher of holes. An optimum
229 photocurrent response is observed with 500 mmol L⁻¹ glucose (see Fig. 6B). When varying the
230 amount of photocatalyst on the electrode surface, 8 μL (or 48 μg) Pt@ZnO on the 3 mm
231 diameter electrode surface appears to provide optimum conditions for maximum photocurrent
232 generation (Fig. 6C).

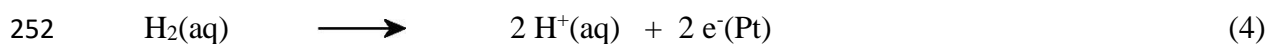
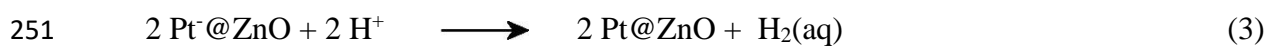
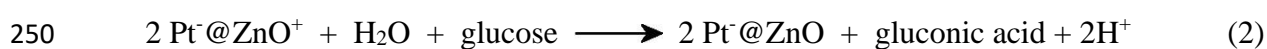
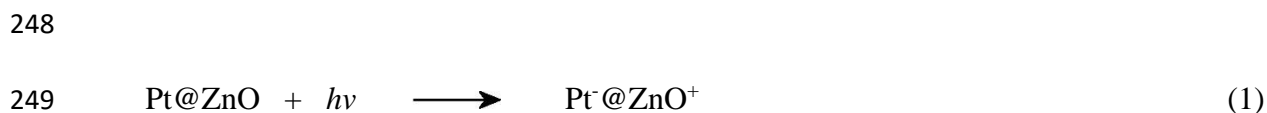
233

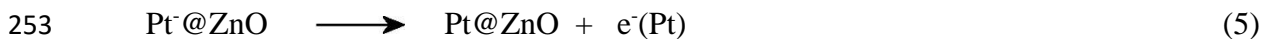
234



235
 236 **Figure 6** – 3D graphic of current vs. potential data from cyclic voltammetry experiments (scan
 237 rate 50 mVs^{-1} ; 3 mm diameter Pt electrode) for different concentrations of glucose in 10 mmol
 238 L^{-1} NaCl with pulse of light of 1s off and 2 s on using a power LED $\lambda = 385 \text{ nm}$ (A). Plot of I_p
 239 vs. concentration of glucose (B). 3D graphic with cyclic voltammetry data for the optimization
 240 of the mass of Pt@ZnO electrode (1 μL equals 6 μg Pt@ZnO) (C).

241
 242 Photocurrents are generated starting at an onset potential of -0.6 V vs. SCE , and a
 243 proposed mechanism can be expressed as a sequence of excitation and charge separation
 244 (equation 1), hole quenching by glucose forming gluconic acid (equation 2), hydrogen
 245 formation (equation 3) and discharge (equation 4). Alternatively, the electrons could diffuse
 246 through the ZnO towards the electrode (equation 5). Similar reaction schemes can be written
 247 either for Pt@ZnO or for ZnO.

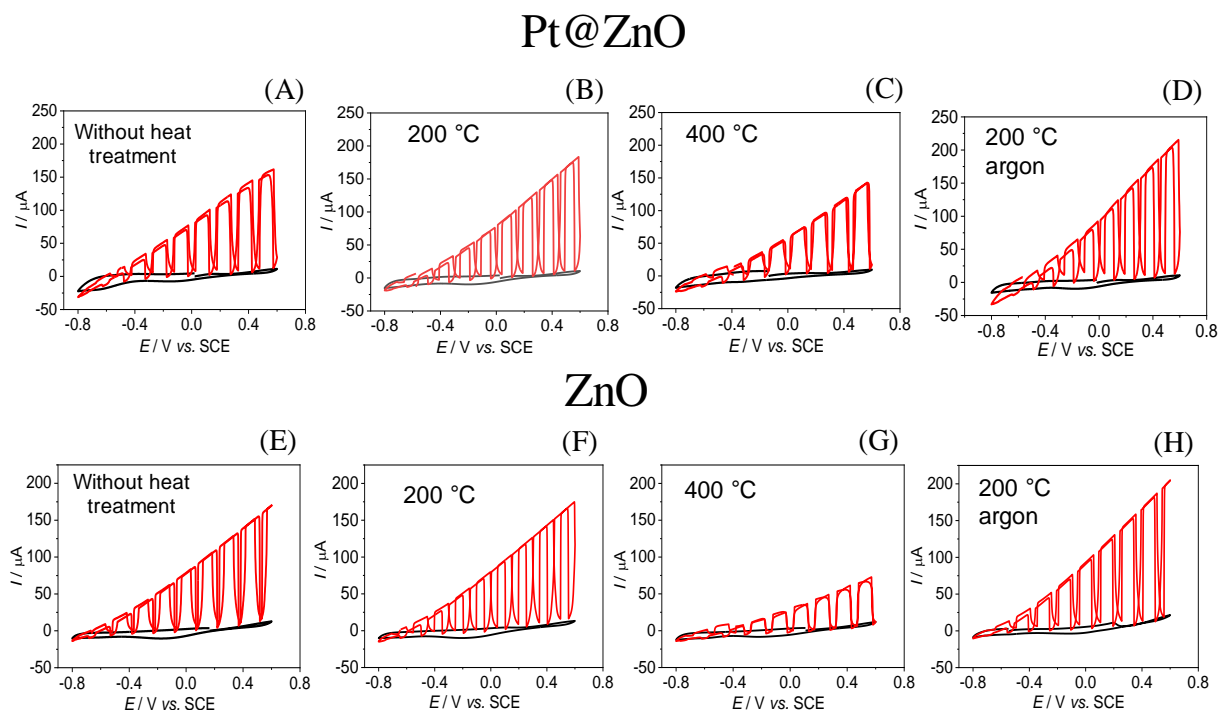




254

255 In order to better understand the underlying processes, both Pt@ZnO and ZnO are
 256 investigated and compared without heat treatment, with 200 and 400 °C heat treatment, and in
 257 the presence of argon/absence of O₂. Data in Fig. 7B and 7F demonstrate that an initial gentle
 258 heat treatment of the photocatalyst powder can be used to stabilise the photo-current responses.
 259 A treatment for 2 h at 200 °C leads to well-defined photocurrents, whereas treatment at 400 °C
 260 (Fig. 7C, G) clearly causes detrimental effects on the photo-redox process. Given that there is
 261 no significant change in the electron optical data for photocatalyst before and after 200 °C heat
 262 treatment, it seems likely that these effects are linked to surface conditioning (dehydration) or
 263 inter-grain contacts. This in turn could affect either chemical/catalytic reactivity of the surface
 264 or electron transport properties across grain boundaries in the ambiently deposited
 265 photocatalysts. Therefore, 200 °C heat treatment can “condition” the ZnO surface to maintain
 266 activity.

267

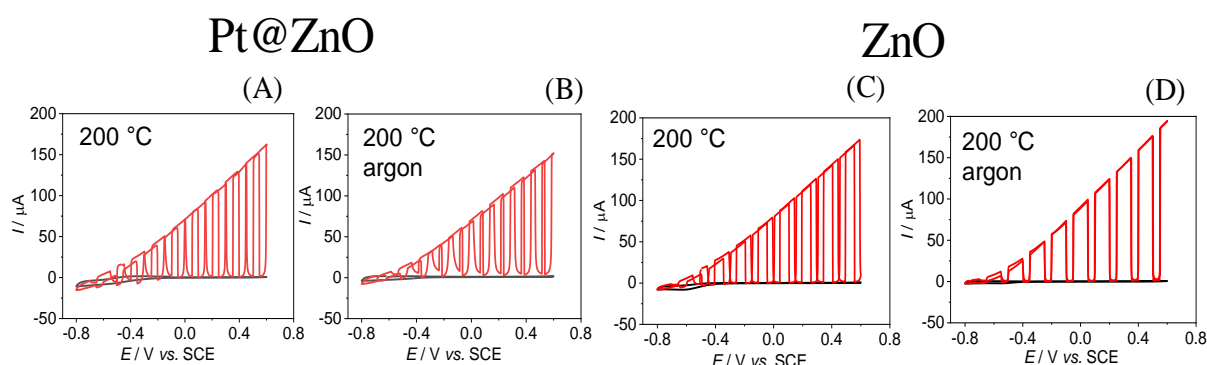


268

269 **Figure 7** – Cyclic voltammety data (scan rate 50 mVs⁻¹; 3 mm diameter Pt electrode) showing
 270 the influence of the heat treatment in the current of the Pt@ZnO/Pt electrode in 10 mmol L⁻¹
 271 NaCl + 500 mmol L⁻¹ glucose without and with pulsed light (1s off and 2 s on; λ = 385 nm) in
 272 air (A-C) and under argon (D). Influence of the heat treatment in the current of the ZnO/Pt
 273 electrode in 10 mmol L⁻¹ NaCl + 500 mmol L⁻¹ glucose without and with pulsed light in air (E-
 274 G) and under argon (H).

275
276
277
278
279
280
281
282
283
284
285
286
287
288
289
290

Fig. 7D and 7H show data for experiments comparing argon de-aerated electrolyte with ambient oxygen containing electrolyte (7B, 7F). Only a minor improvement is observed for both Pt@ZnO and for ZnO photocatalyst materials. This can be attributed to O₂ absence stopping recombination losses with hydrogen or electrons. When investigating the reactivity of ZnO *versus* that of Pt@ZnO the similarity of the photocurrent data is striking. Does the platinum deposit really affect the mechanism under these conditions? Therefore, it is of interest to explore substrate electrodes other than platinum (platinum was chosen initially to capture hydrogen). Fig. 8 shows voltammetry data obtained with pulsed light for Pt@ZnO (A, B) and for ZnO (C, D) deposited on a 3 mm diameter glassy carbon disc electrode and immersed into 10 mmol L⁻¹ NaCl with 500 mmol L⁻¹ glucose. Both the Pt@ZnO and the ZnO photocatalyst give similar photo-current responses. This observation strongly points to a mechanism that doesn't require platinum as catalyst and therefore, the mechanism is based predominantly on electron transport (see equation 4) as opposed to the hydrogen diffusional transport (see equation 3).



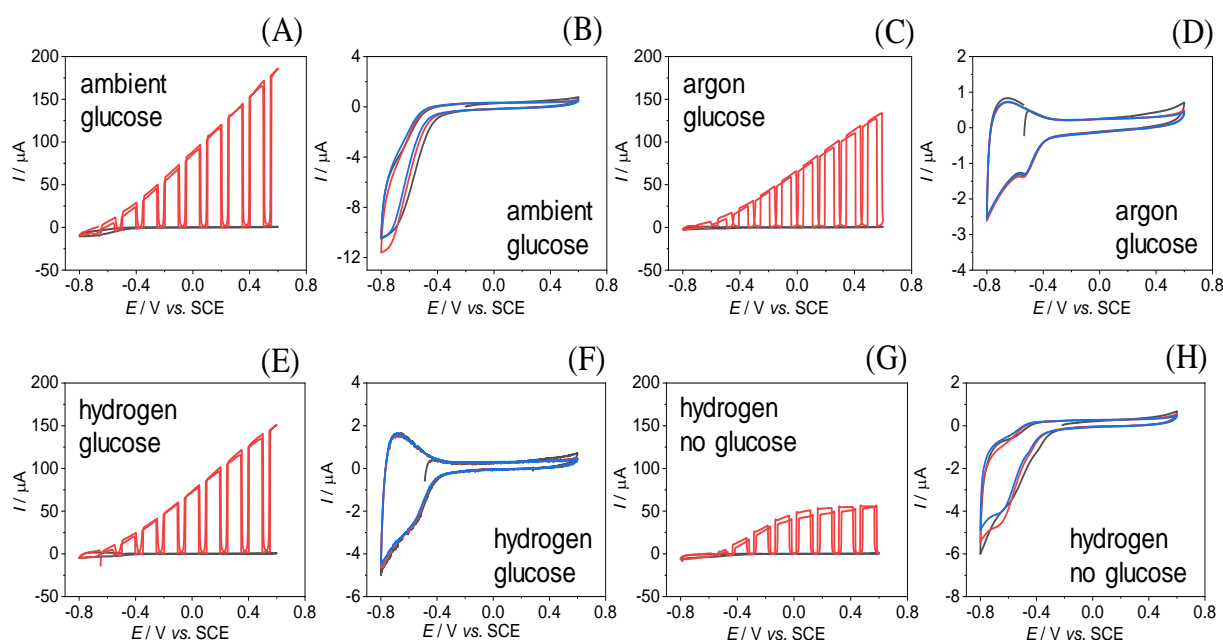
291
292
293
294
295
296
297
298
299
300
301
302

Figure 8 – Current *vs.* potential data from cyclic voltammetry experiments (scan rate 50 mVs⁻¹; 3 mm diameter glassy carbon) for a Pt@ZnO/GC electrode immersed in 10 mmol L⁻¹ NaCl + 500 mmol L⁻¹ glucose without and with pulsed light (1s off and 2 s on; λ = 385 nm) in air (A) and under argon (B). As above, but for a ZnO/GC electrode immersed in 10 mmol L⁻¹ NaCl + 500 mmol L⁻¹ glucose in air (C) and under argon (D).

Further investigation of the mechanism is possible by intentionally purging the solution with hydrogen gas. Data in Fig. 9A show the photo-current responses (red) and the dark current (black) for ZnO on glassy carbon in 10 mmol L⁻¹ NaCl with 500 mmol L⁻¹ glucose. The dark current is shown more clearly in Fig. 9B for potential cycle 1, 5, and 10. The cathodic current shows an onset at approx. -0.6 V *vs.* SCE with a current associated mainly with oxygen

303 reduction. In the presence of argon, the photo-current responses remain similar (Fig. 9C) but
 304 the dark currents are simplified to only the response for the nano-ZnO semiconductor. At a
 305 potential of approx. -0.6 V vs. SCE a cathodic peak is followed by a chemically reversible
 306 reduction/re-oxidation feature consistent with the ZnO surface state reduction and reversible
 307 filling of the ZnO conduction band (in the presence of glucose). This behaviour is retained
 308 under an atmosphere of hydrogen (Fig. 9E, 9F), which clearly shows that hydrogen is not an
 309 intermediate in this process (that is, the process in equation 3 can be ruled out under these
 310 conditions). Hydrogen oxidation (under hydrogen atmosphere) was observed only for the
 311 platinum disc electrodes or for Pt@ZnO coated glassy carbon electrodes (see Fig. S4). The
 312 approximate (poorly defined) equilibrium potential (measured at a platinum disk) for hydrogen
 313 in 10 mmol L⁻¹ NaCl with 500 mmol L⁻¹ glucose was at approx. -0.5 V vs. SCE (see Fig. S4).
 314 Perhaps interestingly, somewhat lower photocurrents are observed also in the absence of
 315 glucose and under hydrogen (Fig. 9G, H) and similar currents are seen also in ambient oxygen
 316 in the absence of glucose (not shown). It can be concluded that some oxygen (either ambient
 317 in solution or generated at the semiconductor surface) can be tolerated in this process. The
 318 somewhat lower plateauing photocurrent and shift in onset potential can be attributed to the
 319 absence of hole quencher.

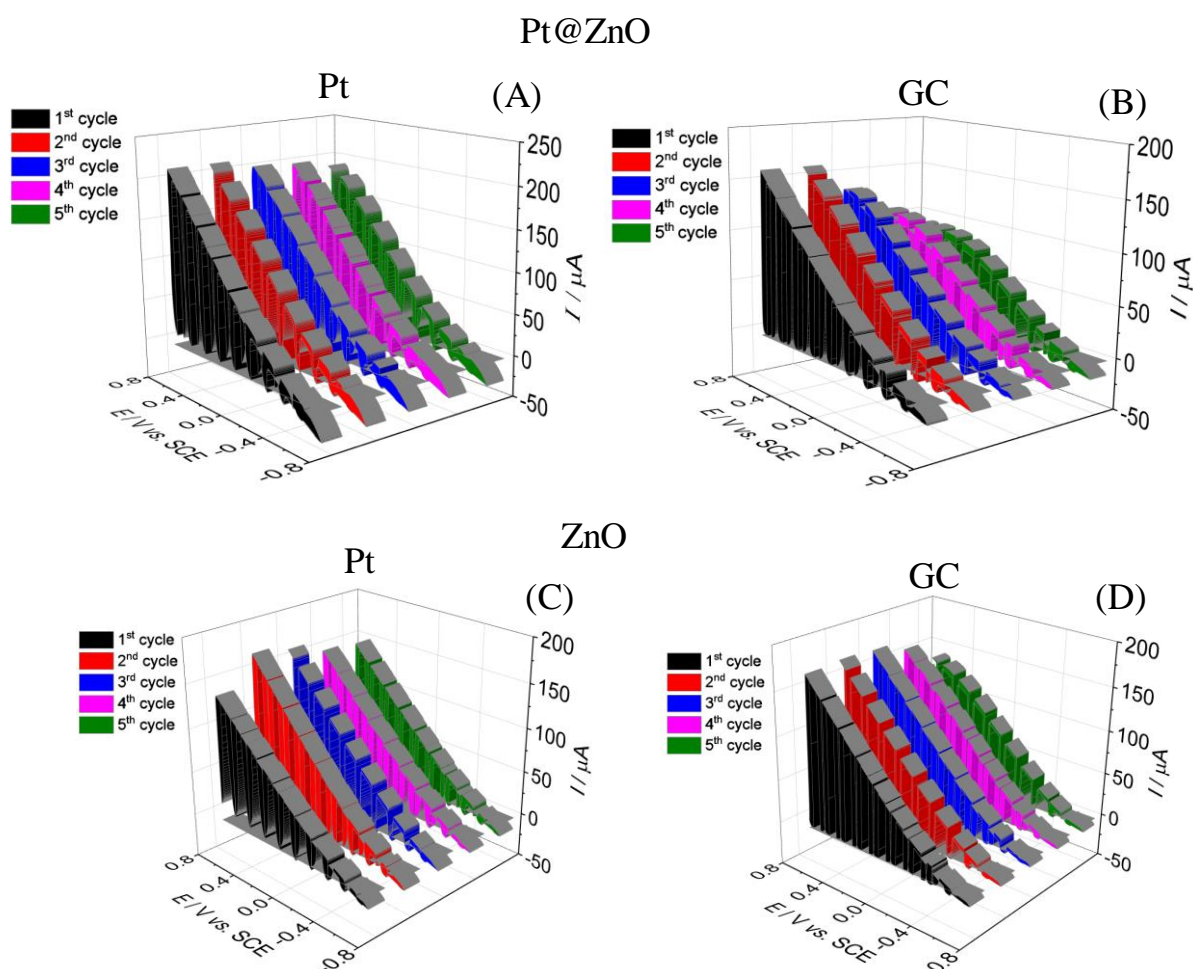
320



321
 322 **Figure 9** – Cyclic voltammetry data (scan rate 50 mVs⁻¹; 3 mm diameter glassy carbon)
 323 showing the influence of environment on the photocurrent for ZnO/GC electrode in 10 mmol
 324 L⁻¹ NaCl + 500 mmol L⁻¹ glucose without and with pulsed light (1s off and 2 s; $\lambda = 385$ nm) in
 325 air (A, B), under argon (C, D), under hydrogen (E, F), and under hydrogen without glucose (G,

326 H). Also shown are cyclic voltammograms without pulse of light (B, D, F and H) 1st cycle (—),
 327 5th cycle (—) and 10th cycle (—).
 328

329
 330 Photocurrent responses from both Pt@ZnO and from ZnO (after 200 °C heat treatment)
 331 are reasonably robust but do decay with prolonged operation (or also for lower glucose
 332 concentrations). Fig. 10 shows data for up to 5 repeat voltammograms for Pt@ZnO and ZnO
 333 and for both glassy carbon and platinum disk electrode substrates. In all cases a gradual change
 334 occurs, and plateauing is observed. Glassy carbon electrodes seem to perform better when
 335 compared to platinum electrodes. Given the surface sensitivity of the overall photo-redox
 336 process, it seems likely that the degradation of the photocurrents is linked to species absorbed
 337 to the ZnO surface. Glucose adsorption itself may play a role and the adsorption of reaction
 338 products such as gluconic acid.
 339



340
 341 **Figure 10** – Cyclic voltammetry (scan rate 50 mVs^{-1} ; 3 mm diameter Pt or GC electrode; using
 342 pulsed light 1s off and 2 s on; $\lambda = 385 \text{ nm}$) for $48 \mu\text{g}$ of Pt@ZnO or ZnO deposits (both with

343 200 °C heat treatment) on the electrode immersed in 10 mmol L⁻¹ NaCl + 500 mmol L⁻¹
344 glucose. (A) Pt@ZnO/Pt, (B) Pt@ZnO/GC, (C) ZnO/Pt, (D) ZnO/GC.

345

346 These data show that the photo-redox process based on photoexcitation of ZnO in the
347 presence of glucose is very similar on both platinum or glassy carbon. Most likely, ZnO after
348 excitation undergoes hole quenching, and then conduction of electrons in ZnO towards the
349 underlying electrode occurs. However, the conduction band electrons from ZnO can still be
350 harvested in the form of hydrogen (*vide infra*). Next, an indirect photoelectrochemical system
351 is investigated based on a palladium membrane electrode. This type of electrode allows the
352 photochemical generation of hydrogen (or conduction band electrons) to be separated from the
353 electrochemical electricity generation. Figure 11A shows a schematic drawing of the indirect
354 photoelectrochemical system.

355

356 **3.3. Indirect Photoelectrochemical Energy Conversion with ZnO and Pt@ZnO** 357 **Nanophotocatalysts**

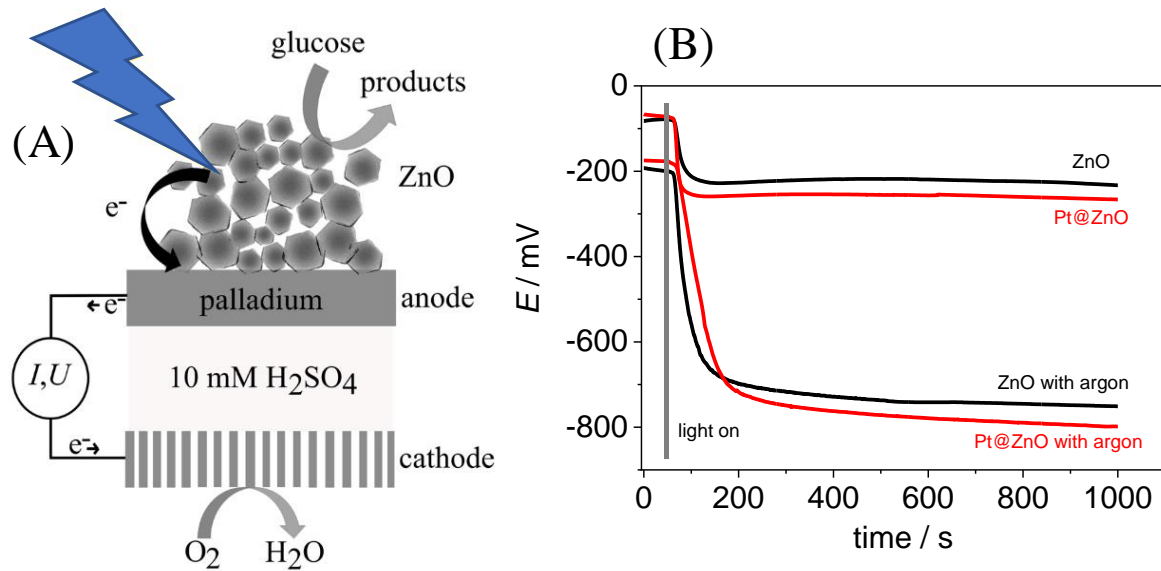
358 Palladium films are known to absorb hydrogen and to allow rapid diffusion of hydrogen across
359 to the opposite side of a thin membrane [15]. Here, a commercial 0.025 mm thick palladium
360 membrane is employed. It has been shown that the diffusion coefficient for hydrogen in
361 palladium or in palladium alloys is approximately $D = 10^{-11} \text{ m}^2 \text{ s}^{-1}$ [19] at room temperature.
362 Therefore, the transport time for hydrogen diffusing through a membrane of thickness $L =$
363 0.025 mm can be estimated as typically $\tau \approx L^2/D \approx 62 \text{ s}$ [20].

364

365 Data in Figure 11B show chronopotentiometry transients for a palladium membrane
366 electrode (exposed area 2 mm diameter) exposed to 500 mmol L⁻¹ glucose in water. Both ZnO
367 and Pt@ZnO provide photo-potential transients within a “switch-on” period of typically 1-2
368 minutes after switching on the light source. In the presence of ambient oxygen or in the
369 presence of argon Pt@ZnO seems to perform slightly better giving a more negative steady state
370 equilibrium potential after a period of 1000 s. The anticipated equilibrium potential for a H₂/O₂
371 electrolytic cell at 1 bar pressure would be 1.23 V [21], but here the oxygen pressure is lower
372 and, more importantly, the hydrogen pressure locally at the palladium surface (facing into the
373 electrochemical cell) is substantially lower due to the binding of hydrogen into the palladium
374 [22]. The presence of oxygen on both sides of the palladium membrane also affects the apparent

375 equilibrium pressure. De-aerating with argon on the electrolyte side where the electrochemical
 376 process occurs (see Figure 12B) improves the photo-potential to approx. -0.8 V, but losses due
 377 to oxygen and the hydrogen concentration gradient through the palladium membrane are still
 378 limiting factors.

379



380

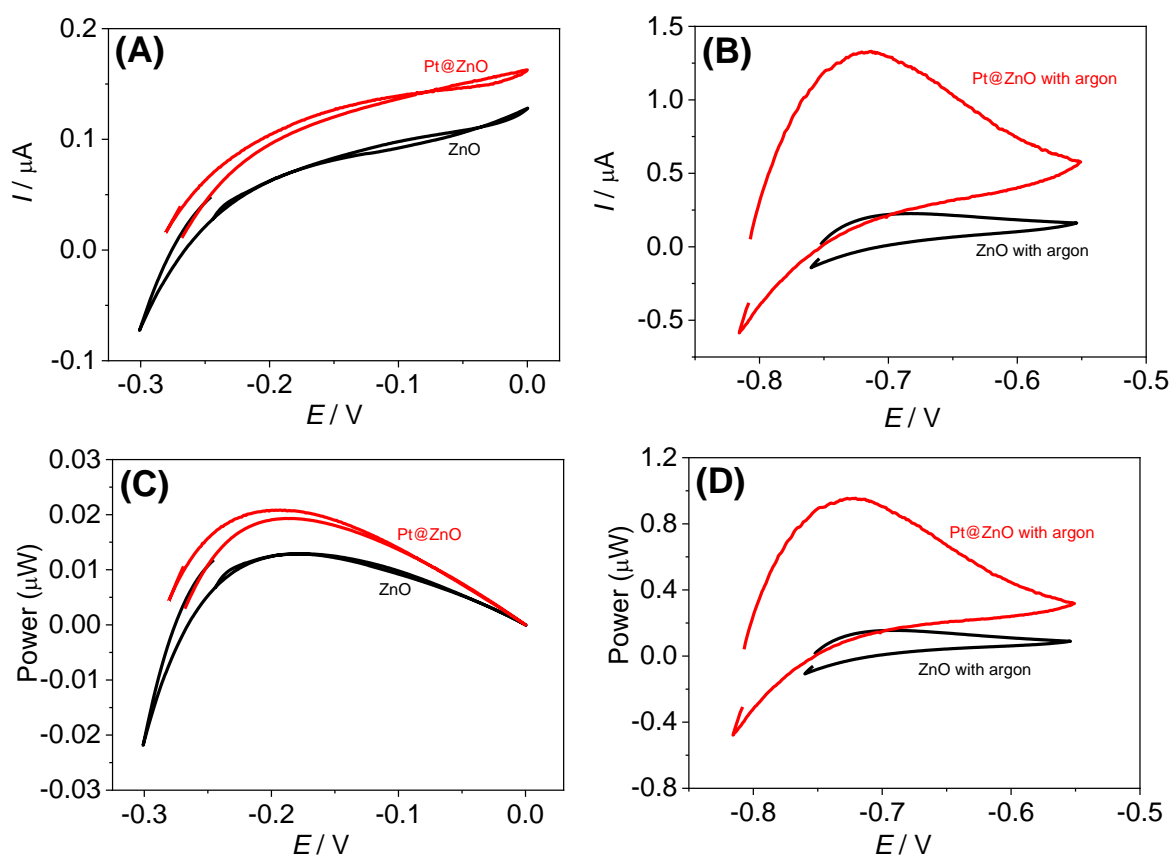
381 **Figure 11** – (A) Schematic drawing of the indirect photoelectrochemical cell with 10 mmol L⁻¹
 382 NaCl and 500 mmol L⁻¹ glucose in the photocatalysis compartment and 10 mmol L⁻¹ H₂SO₄
 383 in the electrochemical compartment. (B) Zero current chronopotentiometry data for 24 μg ZnO
 384 or Pt@ZnO deposited onto a palladium membrane (2 mm diameter) in air and under argon (on
 385 the side of the electrolyte) using a 3D-printed fuel cell (see experimental). Light was switched
 386 on at 50 s.

387

388 The generation of hydrogen at the palladium membrane is clearly detected. The fact that
 389 hydrogen is generated must be linked to the production of electrons in the ZnO deposit (Fig.
 390 11A, *vide supra*). These electrons lower the work-function of the palladium and then lead to
 391 proton uptake to give interstitial hydrogen in the palladium lattice. The overall process can lead
 392 to an indirect photocurrent as is shown in Fig. 12. Fig. 12A shows cyclic voltammetry data
 393 (under constant illumination) and in ambient air conditions. From the apparent equilibrium
 394 potential (OCP) at -0.25 V, the potential is slowly scanned positive (into the power generation
 395 region). The same data when plotted as power *versus* potential (Fig.12C) shows that the
 396 Pt@ZnO photocatalyst performs slightly better with maximum power of 20 nW (or 0.63 μW
 397 cm⁻²). Under argon atmosphere in Fig. 12D (with argon in the electrochemical compartment;
 398 this is more effective compared to purging with argon in the photocatalysis compartment) the

399 cyclic voltammetry response starts at approx. -0.8 V and reaches higher currents, but then
 400 shows depletion effects and a collapse in current at lower voltages. The corresponding power
 401 output peaks at 0.9 μW (or 28 $\mu\text{W cm}^{-2}$). Here, the Pt@ZnO photocatalyst clearly outperforms
 402 the ZnO photocatalyst. The reasons for this and the effects introduced by the palladium
 403 interface will require further study. The rather limited generation of power is likely to be linked
 404 to the performance of the photocatalyst and additional impedance introduced by the palladium
 405 membrane. In the future, improvements will be possible.

406



407 **Figure 12** – (A, B) Cyclic voltammetry (scan rate 1 mVs^{-1}) starting at OCP. A deposit of 24
 408 μg ZnO or Pt@ZnO on a palladium membrane was employed in air (A) and under argon (B).
 409 (C, D) Power plots (power = current \times voltage) due to indirect H_2 generation measured in the
 410 3D-printed photo-fuel cell in air (C) and with argon de-aeration in the electrochemical
 411 compartment (D).
 412

413

414 4. Conclusion

415 It has been shown that commercial nano-ZnO (with approx. 29 nm diameter) ambiently
 416 deposited onto platinum or glassy carbon disc electrodes can be used for photo-current
 417 generation. Glucose added as hole quencher (here employed to mimic biomass) substantially

418 increases the anodic photocurrents, but operation in the absence of glucose (in aqueous 10
419 mmol L⁻¹ NaCl) is also possible. Perhaps surprisingly, both ZnO and Pt@ZnO perform equally
420 well, which is indicative for an electron transport mechanism in ZnO, rather than a hydrogen
421 intermediated mechanism in the surrounding solution. This was further confirmed with
422 experiments performed under hydrogen atmosphere, which allowed formation of hydrogen at
423 the ZnO surface to be ruled out. However, hydrogen was formed when conduction band
424 electrons in ZnO reached the surface of a palladium membrane. This was shown by monitoring
425 photo-potentials and photocurrents in an indirect photo-electrochemical cell. Power-generation
426 was demonstrated. However, more work will be necessary to improve the performance and to
427 better understand the power-limiting photo-current inhibition effects in the mechanism. The
428 ZnO surface seems to play an important role with both glucose adsorption and possibly
429 gluconic acid absorption affecting the processes. More work will be needed to explore the
430 effects of simple molecules such as glucose on the fate of the conduction band electrons in
431 ZnO.

432

433 Indirect photoelectrochemical system are attractive due to the separation of the photocatalysis
434 and the electrolytic power generation. The photocatalytic process when separated does not
435 require electrolyte and could be performed in complex waste media. However, a much better
436 design will be necessary for higher power output and crucially, the palladium membrane needs
437 to be replaced with hybrid materials or composites to perform better and at lower costs. To
438 develop better indirect photo-electrochemical fuel cells in the future, it will be necessary to
439 also develop (A) more stable photocatalysts, (B) improved light absorbers by better interfacial
440 design, and (C) new photocatalysts that allow hydrogen intermediate production and capture
441 under illumination and in the presence of hole quenchers [12]. Hydrogen as a reaction
442 intermediate is more likely to be transferred effectively (from further distance) to the palladium
443 membrane when compared to conduction band electrons in the nanoparticulate ZnO
444 semiconductor.

445

446

447 **Acknowledgements**

448 The authors are grateful to FAPESP (#2014/50945-1) and INCT-DATREN (#465571/2014-0)
449 for support for this work. K.I. received a scholarship from FAPESP (#2019/07020-3).

450

451

452 **References**

- 453 [1] R. Ramachandran, R.K. Menon, An overview of industrial uses of hydrogen, *Int. J.*
454 *Hydrog. Energy.* 23 (1998) 593–598. [https://doi.org/10.1016/S0360-3199\(97\)00112-2](https://doi.org/10.1016/S0360-3199(97)00112-2).
- 455 [2] J.D. Holladay, J. Hu, D.L. King, Y. Wang, An overview of hydrogen production
456 technologies, *Catal. Today.* 139 (2009) 244–260.
457 <https://doi.org/10.1016/j.cattod.2008.08.039>.
- 458 [3] S.N. Paglieri, J.D. Way, Innovations in Palladium Membrane Research, *Sep. Purif.*
459 *Methods.* 31 (2002) 1–169. <https://doi.org/10.1081/SPM-120006115>.
- 460 [4] S. Yun, S. Ted Oyama, Correlations in palladium membranes for hydrogen separation:
461 A review, *J. Membr. Sci.* 375 (2011) 28–45.
462 <https://doi.org/10.1016/j.memsci.2011.03.057>.
- 463 [5] J. Zhang, L. Sun, K. Ichinose, K. Funabiki, T. Yoshida, Effect of anchoring groups on
464 electrochemical self-assembly of ZnO/xanthene dye hybrid thin films, *Phys. Chem.*
465 *Chem. Phys.* 12 (2010) 10494. <https://doi.org/10.1039/c002831b>.
- 466 [6] C. Xia, Z. Qiao, C. Feng, J.-S. Kim, B. Wang, B. Zhu, Study on Zinc Oxide-Based
467 Electrolytes in Low-Temperature Solid Oxide Fuel Cells, *Materials.* 11 (2018) 40.
468 <https://doi.org/10.3390/ma11010040>.
- 469 [7] A.B. Djurišić, X. Chen, Y.H. Leung, A.M.C. Ng, ZnO nanostructures: growth,
470 properties and applications, *J. Mater. Chem.* 22 (2012) 6526–6535.
471 <https://doi.org/10.1039/C2JM15548F>.
- 472 [8] J. Fang, H. Fan, Y. Ma, Z. Wang, Q. Chang, Surface defects control for ZnO nanorods
473 synthesized by quenching and their anti-recombination in photocatalysis, *Appl. Surf.*
474 *Sci.* 332 (2015) 47–54. <https://doi.org/10.1016/j.apsusc.2015.01.139>.
- 475 [9] T. Xu, L. Zhang, H. Cheng, Y. Zhu, Significantly enhanced photocatalytic performance
476 of ZnO via graphene hybridization and the mechanism study, *Appl. Catal. B Environ.*
477 101 (2011) 382–387. <https://doi.org/10.1016/j.apcatb.2010.10.007>.
- 478 [10] Z. Li, Z. Liu, B. Li, D. Li, Y. Fang, Low-loading platinum decorated aligned ZnO
479 nanorods and their photocatalytic and electrocatalytic applications, *J. Mater. Sci. Mater.*
480 *Electron.* 26 (2015) 3909–3915. <https://doi.org/10.1007/s10854-015-2918-2>.
- 481 [11] K. Abdul Razak, S.H. Neoh, N.S. Ridhuan, N. Mohamad Nor, Effect of platinum-
482 nanodendrite modification on the glucose-sensing properties of a zinc-oxide-nanorod
483 electrode, *Appl. Surf. Sci.* 380 (2016) 32–39.
484 <https://doi.org/10.1016/j.apsusc.2016.02.091>.
- 485 [12] (a) Y. Zhao, N.A. Al Abass, R. Malpass-Evans, M. Carta, N.B. McKeown, E. Madrid,
486 P.J. Fletcher, F. Marken, Photoelectrochemistry of immobilised Pt@g-C₃N₄ mediated
487 by hydrogen and enhanced by a polymer of intrinsic microporosity PIM-1, *Electrochem.*
488 *Commun.* 103 (2019) 1–6. <https://doi.org/10.1016/j.elecom.2019.04.006>. (b) Y. Zhao, J.
489 Dobson, C. Harabaiju, E. Madrid, T. Kanyanee, C. Lyall, S. Reeksting, M. Carta, N.B.
490 McKeown, L. Torrente-Murciano, K. Black, F. Marken, Indirect photo-electrochemical
491 detection of carbohydrates with Pt@g-C₃N₄ immobilised into a polymer of intrinsic

- 492 microporosity (PIM-1) and attached to a palladium hydrogen capture membrane,
493 *Bioelectrochem.* 134 (2020) 107499. <https://doi.org/10.1016/j.bioelechem.2020.107499>.
- 494 [13] Y.-K. Hsu, S.-Y. Fu, M.-H. Chen, Y.-C. Chen, Y.-G. Lin, Facile Synthesis of Pt
495 Nanoparticles/ZnO Nanorod Arrays for Photoelectrochemical Water Splitting,
496 *Electrochimica Acta.* 120 (2014) 1–5. <https://doi.org/10.1016/j.electacta.2013.12.095>.
- 497 [14] T. Graham, XXXVI.—On the relation of hydrogen to palladium, *J. Chem. Soc.* 22
498 (1869) 419–432. <https://doi.org/10.1039/JS8692200419>.
- 499 [15] T.L. Ward, T. Dao, Model of hydrogen permeation behavior in palladium membranes, *J.*
500 *Membr. Sci.* 153 (1999) 211–231. [https://doi.org/10.1016/S0376-7388\(98\)00256-7](https://doi.org/10.1016/S0376-7388(98)00256-7).
- 501 [16] R.A. Escalona-Villalpando, A. Dector, D. Dector, A. Moreno-Zuria, S.M. Durón-
502 Torres, M. Galván-Valencia, L.G. Arriaga, J. Ledesma-García, Glucose microfluidic
503 fuel cell using air as oxidant, *Int. J. Hydrog. Energy.* 41 (2016) 23394–23400.
504 <https://doi.org/10.1016/j.ijhydene.2016.04.238>.
- 505 [17] N.A. Al-Shabib, F.M. Husain, F. Ahmed, R.A. Khan, I. Ahmad, E. Alsharaeh, M.S.
506 Khan, A. Hussain, M.T. Rehman, M. Yusuf, I. Hassan, J.M. Khan, G.M. Ashraf, A.
507 Alsalmeh, M.F. Al-Ajmi, V.V. Tarasov, G. Aliev, Biogenic synthesis of Zinc oxide
508 nanostructures from *Nigella sativa* seed: Prospective role as food packaging material
509 inhibiting broad-spectrum quorum sensing and biofilm, *Sci. Rep.* 6 (2016) 36761.
510 <https://doi.org/10.1038/srep36761>.
- 511 [18] R. Herrmann, F.J. García-García, A. Reller, Rapid degradation of zinc oxide
512 nanoparticles by phosphate ions, *Beilstein J. Nanotechnol.* 5 (2014) 2007–2015.
513 <https://doi.org/10.3762/bjnano.5.209>.
- 514 [19] R.V. Bucur, The Influence of Experimental Conditions upon the Measurements of
515 Hydrogen Diffusion in Palladium by Electrochemical Permeation Methods*, *Z. Für*
516 *Phys. Chem.* 146 (1985) 217–229. <https://doi.org/10.1524/zpch.1985.146.2.217>.
- 517 [20] Y. Liu, Y. Li, P. Huang, H. Song, G. Zhang, Modeling of hydrogen atom diffusion and
518 response behavior of hydrogen sensors in Pd–Y alloy nanofilm, *Sci. Rep.* 6 (2016)
519 37043. <https://doi.org/10.1038/srep37043>.
- 520 [21] C. Wei, R.R. Rao, J. Peng, B. Huang, I.E.L. Stephens, M. Risch, Z.J. Xu, Y. Shao-Horn,
521 Recommended Practices and Benchmark Activity for Hydrogen and Oxygen
522 Electrocatalysis in Water Splitting and Fuel Cells, *Adv. Mater.* 31 (2019) 1806296.
523 <https://doi.org/10.1002/adma.201806296>.
- 524 [22] E. McCafferty, Thermodynamics of Corrosion: Pourbaix Diagrams, in: E. McCafferty
525 (Ed.), *Introd. Corros. Sci.*, Springer, New York, NY, 2010: pp. 95–117.
526 https://doi.org/10.1007/978-1-4419-0455-3_6.
- 527